

Lorentz Gas Shear Viscosity via Nonequilibrium Molecular Dynamics and Boltzmann's Equation

Anthony J. C. Ladd¹ and William G. Hoover¹

Received June 19, 1984; revised October 1, 1984

When nonequilibrium molecular dynamics is used to impose isothermal shear on a two-body periodic system of hard disks or spheres, the equations of motion reduce to those describing a Lorentz gas under shear. In this shearing Lorentz gas a single particle moves, isothermally, through a spatially periodic shearing crystal of infinitely massive scatterers. The curvilinear trajectories are calculated analytically and used to measure the dilute Lorentz gas viscosity at several strain rates. Simulations and solutions of Boltzmann's equation exhibit shear thinning resembling that found in N -body nonequilibrium simulations. For the three-dimensional Lorentz gas we obtained an exact expression for the viscosity which is valid at all strain rates. In two dimensions this is not possible due to the anisotropy of the scattering.

KEY WORDS: Boltzmann equation; nonequilibrium; viscosity; molecular dynamics; irreversibility.

1. INTRODUCTION

The Lorentz gas is a simplified model system in which a single particle scatters from fixed scatterers. Usually, the particles are spherical (circular in two dimensions), but other shapes—such as the square “trees” of the Ehrenfests’ “wind-tree” model—can be considered. If the scatterers are not points, then two cases must be distinguished: the scatterers can either overlap, or not.

These Lorentz models are interesting because their properties can be understood theoretically. They have been used to elucidate the difficulties

¹ Department of Applied Science, University of California at Davis, California 95616 and Lawrence Livermore National Laboratory Livermore, California 94550.

that arise in attempting to extend the Boltzmann equation to "higher" (nonzero) densities.²

Here we consider a simpler case in which only two hard particles are involved, disks in two dimensions or spheres in three dimensions. Since there is only one scatterer the possibility of scatterer overlap does not occur. The problem is made interesting by adding periodic boundary conditions (see Fig. 1) so that each particle scatters from a periodic lattice of images of the other particle.

For hard particles only the sum of the radii matters so that the system can be viewed as consisting of two particles with radii $\sigma/2$ or one particle of radius σ and a point particle. Likewise, the system can be viewed from a frame fixed in space, so that both particles move in a symmetric way, with velocities v and $-v$. Alternatively the same system can be viewed from a frame fixed on one of the particles. The other particle then moves at a velocity $2v$.

² See Refs. 1 and 2. Reference 1 briefly lists the physical applications of the Lorentz model (electrons, neutrons, and mixtures) and then gives a comprehensive summary of the underlying theory.

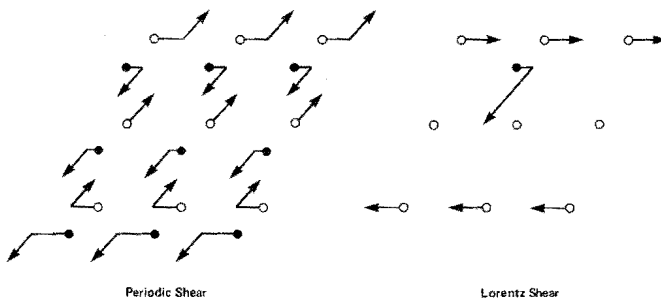


Fig. 1. Two-body periodic isothermal shear flow, the simplest system illustrating thermodynamic irreversibility. Two equal-mass particles are shown at the left. The inertial-frame velocities are shown as sums of a systematic strain-rate contribution (horizontal) and a thermal part. Both particles move at a speed $(2kT/m)^{1/2}$. The equivalent Lorentz gas system is shown at the right. The infinitely massive scattering particle moves horizontally, with only the systematic strain-rate velocity, $\dot{\epsilon}y$. The scattering particle, with mass $m/2$, moves with twice the speed of the particles shown at the left. In either case the motion is governed by Eq. (1) of the text. In drawing the figure the open circle particle lies at $y=0$ so that its systematic velocity is zero. The systematic velocities of its images above and below are $+\dot{\epsilon}L$ and $-\dot{\epsilon}L$, respectively. L is the repeat distance between images and $\dot{\epsilon}$ is the strain rate du_x/dy . The other particle, shown as a filled circle, has a systematic (horizontal) velocity proportional to its y coordinate as well as a thermal velocity equal to the negative of that of the open-circle particle. On the right (Lorentz) side of the figure the velocities are measured relative to a *fixed* open circle. In this coordinate frame the filled circle again has a systematic velocity $\dot{\epsilon}y$ and has an additional "thermal" velocity $-2v$.

Here we focus on the viscosity of the two-body system. This is the simplest realization of "nonequilibrium molecular dynamics" techniques developed over the past decade for application to many-body systems. As is described in the next section, the same equations can be applied to two bodies, and the low-density viscosity thus obtained is a reasonably faithful caricature of the many-body result obtained from the Boltzmann equation.

"Exact" numerical diffusion-coefficient results have already been obtained, by equilibrium molecular dynamics computer simulation, for both overlapping and nonoverlapping Lorentz gas scatterers.⁽³⁻⁵⁾ The results generally justify the conclusions of kinetic theory, with respect to the long-time behavior of the velocity autocorrelation function and the diffusion coefficient D . In either two or three dimensions, with randomly distributed points scattering a hard disk or sphere, the coefficient D varies nonanalytically with scatterer density: $D \sim 1/\rho + O(\ln \rho)$ in two dimensions, and $1/\rho + O(1) + O(\rho \ln \rho)$ in three dimensions. Numerical simulation is consistent with these logarithmic terms and shows that, overall, D varies rather smoothly with density.

Nonequilibrium molecular dynamics has progressed rapidly over the last decade.⁽⁶⁾ The early reservoir techniques were quickly replaced by periodic homogeneous simulations utilizing modifications of Newton's equations of motion. All of the methods used appear to be self-consistent when number dependence and rate dependence are taken into account. Detailed comparisons have demonstrated the agreement, at low strain rates, of the nonequilibrium methods with the formally exact Green-Kubo fluctuation approach.⁽⁷⁾ Although most simulation work has focused on determining the linear transport coefficients, diffusion, viscosity, and heat conductivity, even monatomic fluids have been found to exhibit the complex strain-rate-dependent rheology characteristic of polymeric fluids. The rates involved, for the monatomic fluids, in the gigahertz to terahertz range, exceed those for which laboratory measurements can conveniently be made. There is no doubt, however, that even higher rates exist in the shockwaves generated by explosives.⁽⁸⁾

Here we consider the strain-rate-dependent shear viscosity of the Lorentz gas. This is the simplest system to which the equations of nonequilibrium molecular dynamics can be applied. Because the system can be described in a three-dimensional phase space (albeit with a density in that space which is periodic in time) it is the simplest system illustrating thermodynamic dissipation and irreversibility as well as nonlinear rate-dependent viscosity.

It is difficult to decide, *a priori*, whether or not the nonlinear flow behavior resulting in normal stresses and shear thinning can be meaningfully characterized by computer simulations and related to real

measurements.³ In an attempt to shed light on this question we have examined the shear flow in a dilute gas described by the equations of motion of nonequilibrium molecular dynamics,⁽¹⁰⁾ via nonlinear solutions of the relaxation-time Boltzmann equation. We compare the distribution functions and transport coefficients from our nonequilibrium equations of motion with those obtained more conventionally, with boundary-driven flows. We find that the isothermal equations of motion generate the correct one-particle distribution function for steady Couette flow to all orders in the strain rate.

In Section 2 we describe the nonequilibrium equations of motion and apply them to Lorentz gas trajectories. In Section 3 we give results for the model from computer simulation. In Section 4 we solve Boltzmann's equation for both the two-body Lorentz gas and the many-body models of nonlinear Couette flow. In Section 5 we discuss the thermodynamic irreversibility associated with the Lorentz gas.

2. NONEQUILIBRIUM EQUATIONS OF MOTION AND LORENTZ GAS TRAJECTORIES

Particles undergoing a spatially periodic shear at constant temperature can be described by the nonequilibrium equations of motion recently reviewed by Evans and Morris⁽¹⁰⁾

$$\begin{aligned}\dot{x} &= (p_x/m) + \dot{\epsilon}y, & \dot{y} &= (p_y/m), & \dot{z} &= (p_z/m) \\ \dot{p}_x &= F_x - \dot{\epsilon}p_y - \zeta p_x, & \dot{p}_y &= F_y - \zeta p_y, & \dot{p}_z &= F_z - \zeta p_z \\ \dot{\epsilon} &\equiv du_x/dy, & \zeta &\equiv \sum [(F \cdot p - \dot{\epsilon}p_x p_y)/m] / \sum (p^2/m)\end{aligned}\quad (1)$$

The "thermal velocity" p/m is measured *relative* to the fixed stream velocity $\dot{\epsilon}y$. The "friction coefficient" ζ varies with time (through its dependence on the forces and momenta) in such a way that the kinetic energy $\sum p^2/2m$ (proportional to temperature) is a constant of the motion. An alternative constraint, identical between collisions, is to maintain a constant internal energy ($\sum p^2/2m + \Phi$).

A variant of Eqs. (1), the "Doll's tensor" equations of motion,⁽¹¹⁾ results if the x and y subscripts in the second line are permuted. Either set of equations, (1) or the Doll's tensor analog, produces the correct low-strain-rate viscosity. The exploratory calculations listed in Tables Ia and Ib indicate that the normal stresses given by the two sets are different though they are unaffected by the choice of isoenergetic or isothermal constraints.

³ This question is discussed at length in Ref. 9.

Table 1a. Kinetic Contribution to the Shear Viscosity and Normal Stress Coefficients at a Density $\rho = N\sigma^3/\sqrt{2V} = 0.4$, Temperature $kT/\epsilon = 1$, and Strain Rate $\dot{\epsilon}(m\sigma^2/kT)^{1/2} = 1$, by Various Nonequilibrium Molecular Dynamics Methods.

Method ^a	$\eta^K \sigma^2(mkT)^{-1/2}$	$\Psi_1^K(\sigma/m)$	$\Psi_2^K(\sigma/m)$
1	0.11	0.03	-0.04
2	0.11	-0.03	-0.01
3	0.11	-0.04	-0.00
4	0.13	-0.04	-0.21

^a Method 1, Doll's tensor + isoenergetic constraint; method 2, correct Coriolis force + isoenergetic constraint; method 3, correct Coriolis force + isothermal constraint; method 4, correct Coriolis force + isothermal constraint in T_{zz} only. Each simulation involved 32 particles interacting via an inverse 12th-power potential, $\phi = \epsilon(\sigma/r)^{12}$, with a run time of 600 $(m\sigma^2/kT)^{1/2}$. The viscosity and normal stress coefficients, Ψ_1 and Ψ_2 , are defined by (see article by R. B. Bird in Ref. 9). "Correct Coriolis force" corresponds to Eq. (1).

$$\eta = -P_{xy}/\dot{\epsilon}, \quad \Psi_1 = -(P_{xx} - P_{yy})/\dot{\epsilon}^2, \quad \Psi_2 = -(P_{yy} - P_{zz})/\dot{\epsilon}^2$$

The error bars are within the quoted accuracy.

Table 1b. Molecular Dynamics Simulations of Couette Flow at a Density, $\rho = N\sigma^3/\sqrt{2V} = 0.6$, Temperature $kT/\epsilon = 1$, and Strain Rate $\dot{\epsilon}(m\sigma^2/kT)^{1/2} = 1$, for an Inverse 12th-Power Potential

Method ^a	N	$P\sigma^3/kT$	$\eta\sigma^2(mkT)^{-1/2}$	$\Psi_1(\sigma/m)$	$\Psi_2(\sigma/m)$
<i>T</i>	32	8.28	1.21	0.16	-0.19
<i>E</i>	32	8.27	1.21	0.16	-0.19
<i>E</i>	108	8.25	1.22	0.04	-0.16
<i>E</i>	256	8.26	1.23	0.04	-0.16

^a Both isoenergetic (*E*) and isothermal (*T*) molecular dynamics were used corresponding to methods (2) and (3) of Table 1a, respectively. Between 32 and 256 particles were used with run times of 500 to 5000 $(m\sigma^2/kT)^{1/2}$. The error bars are approximately one in the last quoted figure.

We discuss later, in Section 4, an argument based on the Boltzmann equation which suggests that the set (1) is more nearly correct for determining normal stresses.

It is not obvious whether or not Eqs. (1) have stable solutions for small systems. But numerical integration indicates that solutions are stable for periodic systems of only two or three particles. In mathematical terms,

a two-body periodic system is identical to a Lorentz gas with spatially periodic scatterers. To see this, choose a coordinate system fixed on one particle in a two-body system (see Fig. 1). Then substitute $R \equiv r_1 - r_2$, $P \equiv p_1$, and $M = m/2$ into Eqs. (1). Exactly the same equations (1) result, but with the lower-case variables r , p , m replaced by R , P , M , where M is the reduced mass (μ). For clarity we will emphasize the two-dimensional hard-disk analog of the equations above. Thus, if the total internal energy of the two-body system is $2kT \equiv \sum p^2/2m = p^2/m$, the internal energy of the equivalent Lorentz gas is also $2kT$ ($3kT$ in three dimensions). The moving Lorentz particle has twice the speed of either two-body particle, but only half the mass.

Between collisions, when the force F vanishes, Eqs. (1) can be integrated analytically. This gives curvilinear trajectories which are segments—beginning and ending with collisions—of curves of the type shown in Fig. 2. The two-dimensional case is worked out in detail in Appendix A. It is important to realize that the isothermal restriction ($p^2/2m = \text{const}$) on the trajectories forces the wandering particle to move at a velocity similar to that of nearby scatterers. Because the y coordinate diverges gradually (as $\pm \ln t$ for t large) there is no possibility of avoiding eventual collision, which transfers the wandering particle to a new section of the universal trajectory of Fig. 2.

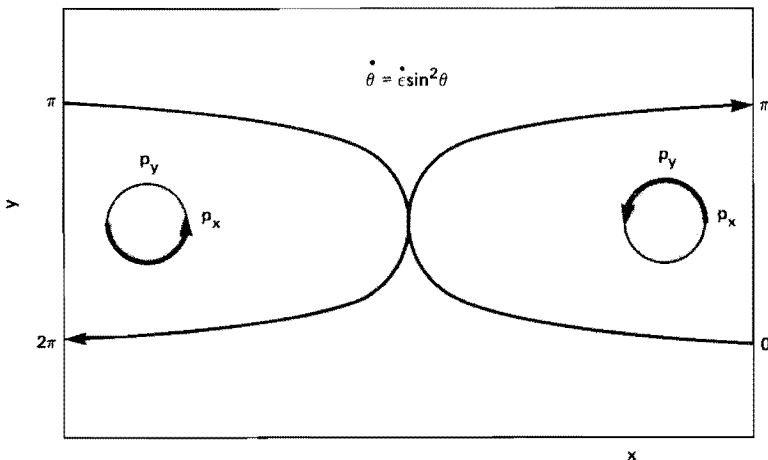


Fig. 2. Trajectory followed between collisions according to the isothermal shear flow equations (1). The scale of the figure varies inversely with the strain rate $\dot{\epsilon}$. A particle moving upward ($p_y > 0$) follows the c-shaped curve from lower right to upper right, first leading the flow ($p_x > 0$) and later lagging behind it ($p_x < 0$). A particle moving downward ($p_y < 0$) travels in the reverse direction along the mirror-image curve.

The collisional momentum transfer is complicated by the isothermal restriction. In these calculations, both computer simulation and Boltzmann equation, we have assumed that the product of the strain rate and collision cross section is much smaller than the thermal velocity. The collisions are then the same as in the equilibrium case. At higher densities and strain rates Eqs. (1) must be integrated through the collision numerically, for some suitable potential, using either an isothermal or isoenergetic constraint. A very steep repulsive Hooke's law force is suitable for this purpose.

3. NONEQUILIBRIUM MOLECULAR DYNAMICS

The shearing two-body periodic system was simulated over the range of strain rates $\dot{\epsilon} = du_x/dy$ shown in Table II. The calculation proceeds by calculating the time at which the wandering particle next encounters a strip $(n\sqrt{V} - \sigma) < y < (n\sqrt{V} + \sigma)$ in which collisions with particles at $x_{mn} = m\sqrt{V} + \dot{\epsilon}tn\sqrt{V}$ might occur. Any such collision is located iteratively; the contributions to the pressure tensor are tallied; the new postcollision velocity is determined, and the process is repeated. Runs of several million collisions are feasible and yield pressure tensors and viscosities,

$$\begin{aligned} PV &\equiv \sum pp/m + \sum r_{ij}F_{ij} \\ \eta &\equiv -P_{xy}/\dot{\epsilon} \end{aligned} \quad (2)$$

accurate to about one part in a thousand.

Table II. Molecular Dynamics Simulations of the Two-Dimensional Viscous Lorentz Gas, at a Volume $V=100\sigma^2$

$\dot{\epsilon}\sigma(m/kT)^{1/2}$	N_{coll}	$(\dot{\epsilon}\tau)$	η/η_B
0.0003	9.7×10^6	0.00514	1.07(11)
0.001	2.5×10^6	0.0171	0.93(6)
0.003	2.5×10^6	0.0514	0.77(3)
0.01	1.0×10^6	0.171	0.78(1)
0.03	0.5×10^6	0.512	0.71(1)
0.1	0.2×10^6	1.62	0.39(0)

^a The viscosity is calculated relative to the zero strain rate, zero density viscosity obtained from a solution of the Boltzmann equation, $\eta_B = 0.161(mkT/\sigma^2)^{1/2}$. The zero strain rate collision time is given by $1/\tau = 4\sigma(kT/\mu)^{1/2}/(V - \pi\sigma^2)$, and contains the excluded volume correction.

The low-density, small-strain-rate viscosity can be obtained from Boltzmann's equation, as shown in Section 4. The computer results appear to approach this limit

$$\begin{aligned}\eta_0 \sigma / (mkT)^{1/2} &= 15 \sqrt{2}/128 = 0.166 && (\text{disks}) \\ \eta_0 \sigma^2 / (mkT)^{1/2} &= \sqrt{3}/5\pi = 0.110 && (\text{spheres})\end{aligned}\quad (3)$$

Gass⁽¹²⁾ quotes Senger's many-body disk result, $(4\pi)^{-1/2} = 0.282$, about 70% greater. The corresponding reduced hard-sphere viscosity, 0.176, likewise considerably exceeds the two-body value. At higher rates the viscosity eventually vanishes and the pressure tensor approaches the limiting form (in two dimensions)

$$\mathbf{P} \rightarrow \begin{bmatrix} 2 & 0 \\ 0 & 0 \end{bmatrix} NkT/V$$

It appears that the viscosity vanishes at least as strongly as $\dot{\varepsilon}^{-3/2}$ for high rates, but we have not been able to prove this.

4. BOLTZMANN'S EQUATION

Boltzmann's equation can be applied to the Lorentz-gas model with the velocity-dependent forces in a straightforward way. If we describe the thermal velocity $p/m = \dot{r} - (\hat{e}_y, 0)$ using plane polar coordinates:

$$\begin{aligned}p_x &= p \cos \theta \\ p_y &= p \sin \theta\end{aligned}\quad (4)$$

then the equation of motion (1) has the form

$$\dot{\theta} = \dot{\varepsilon} \sin^2 \theta \quad (5)$$

Boltzmann's equation becomes

$$\frac{\partial f}{\partial t} + \frac{\partial}{\partial \theta} (f \dot{\theta}) = \left(\frac{\partial f}{\partial t} \right)_{\text{collisions}} \quad (6)$$

The relaxation-time model replaces the collision term by $(f_0 - f)/\tau$, where $f_0 = 1/2\pi$ so that $\int f d\theta \equiv 1$. For the two-body periodic system the collision rate $1/\tau$ is $2\sigma(8kT/m)^{1/2}/V$. For the equivalent one-body analog, $1/\tau$ is $2\sigma(4kT/\mu)^{1/2}/V = 4\sigma(kT/\mu)^{1/2}/V$ where $\mu = m/2$. Thus the linear steady state solution of the relaxation-time model $f = f_0 + \tau f_1$ can be obtained from

$$\frac{\partial}{\partial \theta} (f_0 \dot{\varepsilon} \sin^2 \theta) = \frac{\dot{\varepsilon}}{\pi} \sin \theta \cos \theta = (f_0 - f)/\tau = -f_1 \quad (7)$$

In two dimensions the scattering is anisotropic. The "collision operator" distributes f with a probability density equal to $(1/4) |\sin(\delta\theta/2)|$ and the collision integral can be worked out analytically,

$$\left(\frac{\partial f}{\partial t} \right)_{\text{collisions}} = \frac{1}{4\tau} \int_{-\pi}^{\pi} \{f(\theta - \delta\theta) - f(\theta)\} |\sin(\delta\theta/2)| d(\delta\theta) \quad (8)$$

A Chapman-Enskog expansion indicates that

$$f_1 \propto \sin 2\theta \quad (9)$$

and an exact collision-term calculation reduces the perturbation f_1 by a factor of $15/16$. The viscosity obtained by averaging over the steady state distribution function, f_1 , is given in Eq. (3).

We solved the two-dimensional nonlinear equation (6) numerically by iterating a centered-difference version to a steady state for 4, 8, 16, 32, 64, and 128 intervals in θ . The results indicate errors varying as the inverse square of the number of intervals. This estimate was used to compute the viscosities listed in Table III and appearing in Fig. 3. An asymptotic expansion establishes that the viscosity varies quadratically at low strain rates:

$$\frac{\eta}{\eta_0} = 1 - (\dot{\varepsilon}\tau)^2 + O(\dot{\varepsilon}\tau)^4 \quad (10)$$

Table III. Viscosities from the Nonlinear Boltzmann Equation for a Periodic Two-Body System

$\dot{\varepsilon}\sigma(m/kT)^{1/2}$	$(\dot{\varepsilon}\tau)$	η/η_0
0.000	0.0000	1.0000
0.001	0.0177	0.9996
0.01	0.177	0.9630
0.02	0.354	0.8837
0.05	0.884	0.6450
0.10	1.77	0.4069
0.20	3.54	0.2096

^a The data were obtained using a collision rate appropriate to a volume of $100\sigma^2$. Both particles have mass m and speed $(2kT/m)^{1/2}$. To convert the strain rates given to the dimensionless form $\dot{\varepsilon}\tau$ where $1/\tau$ is the mean two-body collision rate multiply the rates quoted by $25\sigma/(2kT/m)^{1/2}$. The low-density zero-rate viscosity $\eta_0 \equiv 15(2mkT)^{1/2}/128\sigma = 0.166(mkT/\sigma^2)^{1/2}$.

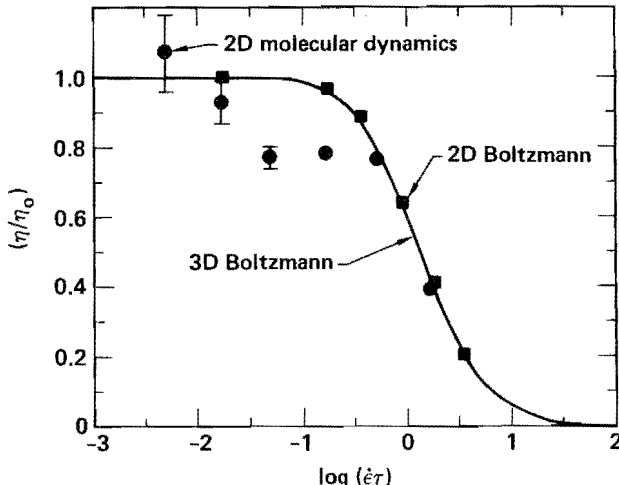


Fig. 3. Strain-rate dependent low-density viscosities. The solid line is the solution of the three-dimensional Boltzmann equation [Eq. (19)]. The squares are solutions of the two-dimensional Boltzmann equation [Eq. (6)]. The results are scaled by the zero-frequency viscosity and the mean collision time. The circles are the results of the two-dimensional molecular dynamics simulations. The error bars, shown when greater than the size of the circles, are one standard error.

The predictions of the two-dimensional Boltzmann equation can be compared with the results of numerical simulation (Table II) as shown in Fig. 3. The two calculations are consistent at low strain rates, but the simulation results have a larger and more complex dependence on strain rate. The reason for this is unclear. In solving the Boltzmann equation we have assumed that the collision time is independent of the direction of the velocity. The indication both from theory and simulation are that this assumption is true, at least at low strain rates. The variation in mean free path between strips $l = V^{1/2}/\sin \theta$ is exactly canceled by the angle-dependent probability of collision as the particle crosses a strip. For a single strip, $P = 2\sigma/(V^{1/2} \sin \theta)$. For small angles, $\theta < 2\sigma/V^{1/2}$, a collision is certain, but this is a negligible effect at low densities. The cumulative mean free path is

$$l/P + 2l/P(1-P) + 3l/P(1-P)^2 + \dots = l/P = V/2\sigma \quad (11)$$

and thus the collision time is independent of the velocity direction θ .

In the three-dimensional case the analysis is likewise simplified by introducing spherical polar coordinates

$$p_x = p \cos \phi, \quad p_y = p \sin \phi \cos \theta, \quad p_z = p \sin \phi \sin \theta \quad (12)$$

Between collisions the equations of motion are

$$\dot{\theta} = 0, \quad \dot{\phi} = \dot{\epsilon} \sin^2 \phi \cos \theta \quad (13)$$

The scattering is isotropic, and the low-density linear perturbation to the distribution function is exactly

$$(f_0 - f)/\tau = -f_1 = 3\dot{\epsilon} \sin \phi \cos \phi \cos \theta f_0 \quad (14)$$

where the collision rate $1/\tau$ is $\pi\sigma^2(12kT/m)^{1/2}/V$.

The nonlinear Boltzmann equation takes the relatively simple form,

$$\begin{aligned} \frac{df}{dt} = \frac{\partial}{\partial p} \cdot (\dot{p}f) &= \dot{\epsilon} \cos \theta \left(\sin^2 \phi \frac{\partial f}{\partial \phi} + 3 \sin \phi \cos \phi f \right) \\ &= -(f - f_0)/\tau \end{aligned} \quad (15)$$

which has a solution in the spherical polar coordinates defined in Eq. (12),

$$f = (4\pi)^{-1} (1+x^2)^{3/2} \sum_{n=0}^{\infty} (\dot{\epsilon}\tau \cos \theta)^n \frac{\partial^n}{\partial x^n} (1+x^2)^{-3/2} \quad (16)$$

where $x = \cot \phi$. The distribution function can be expressed in terms of a forward and backward Fourier transform in the variable x ,

$$f = \frac{1}{8\pi^2} (1+x^2)^{3/2} \int_{-\infty}^{\infty} dq e^{ixq} \sum_{n=0}^{\infty} (iq\dot{\epsilon}\tau \cos \theta)^n \int_{-\infty}^{\infty} dx' e^{-iqx'} (1+x'^2)^{-3/2} \quad (17)$$

and the viscosity can be obtained from the appropriate moment of f ,

$$\begin{aligned} \eta &= -\frac{1}{\dot{\epsilon}V} \int_0^\pi \sin \phi d\phi \int_0^{2\pi} d\theta \frac{p^2}{\mu} \sin \phi \cos \phi \cos \theta f \\ &= (p^2/\mu\dot{\epsilon}V) \int_0^\infty e^{-q} (\dot{\epsilon}\tau q)^{-1} \{1 - (1 + [\dot{\epsilon}\tau q]^2)^{-1/2}\} q K_1(q) dq \end{aligned} \quad (18)$$

where K_1 is a modified Bessel function. By expanding the algebraic term in the integrand, an asymptotic series for the low strain rate limit is obtained:

$$\begin{aligned} \eta/\eta_0 &= 5(\dot{\epsilon}\tau)^{-2} \int_0^\infty \{1 - (1 + [\dot{\epsilon}\tau q]^2)^{-1/2}\} e^{-q} K_1(q) dq \\ &= 1 - \frac{10}{7} (\dot{\epsilon}\tau)^2 + \frac{1000}{143} (\dot{\epsilon}\tau)^4 \dots \end{aligned} \quad (19)$$

At higher strain rates, the integral can be evaluated numerically, by Gauss-Laguerre quadrature, and the results are shown in Fig. 3. The two-dimensional and three-dimensional low-density viscosities have a very similar dependence on shear rate.

The Boltzmann equation can also be analyzed for a many-body (as opposed to one- or two-body) system. In this case, the "friction coefficient" ζ is not a dynamical variable, but is found by requiring that there be no net increase in internal energy

$$\zeta(\dot{\epsilon}) = -\dot{\epsilon} \langle p_x p_y \rangle / \langle p^2 \rangle \quad (20)$$

In the relaxation-time approximation it is again possible to expand the distribution function, this time around the limiting Maxwell-Boltzmann f_0 :

$$f = f_0 + \tau f_1 + \tau^2 f_2 + \tau^3 f_3 + \tau^4 f_4 + \dots \quad (21)$$

The solution predicts shear thinning:

$$P_{xy} V/NkT = \frac{-(\dot{\epsilon}\tau) + 2(\dot{\epsilon}\tau)^3 - \dots}{-(\dot{\epsilon}\tau) + (4/3)(\dot{\epsilon}\tau)^3 - \dots}, \quad \begin{array}{l} \text{(disks)} \\ \text{(spheres)} \end{array} \quad (22)$$

agreeing with Zwanzig's hard-sphere analysis,⁽¹³⁾ and dilatancy

$$(P_{xx} - P_{yy}) V/NkT = 2(\dot{\epsilon}\tau)^2 - 6(\dot{\epsilon}\tau)^4 + \dots, \quad \begin{array}{l} \text{(disks)} \end{array} \quad (23)$$

$$(P_{xx} - P_{yy}) V/NkT = (P_{xx} - P_{zz}) V/NkT = 2(\dot{\epsilon}\tau)^2 - 4(\dot{\epsilon}\tau)^4 + \dots, \quad \begin{array}{l} \text{(spheres)} \end{array}$$

agreeing with Chapman and Cowling's result.⁽¹⁴⁾ The entropy, defined in terms of the average value of $\ln f$, is reduced by the shear flow, but, as expected on physical grounds, by less than the prediction from the quadratic term alone:

$$\Delta S/Nk = \frac{-(\dot{\epsilon}\tau)^2/2 + 3(\dot{\epsilon}\tau)^4/4 - \dots}{-(\dot{\epsilon}\tau)^2/2 + (\dot{\epsilon}\tau)^4/4 - \dots}, \quad \begin{array}{l} \text{(disks)} \\ \text{(spheres)} \end{array} \quad (24)$$

A similar analysis can be carried out using the Doll's tensor equations of motion, which treat Coriolis accelerations differently, or for alternative equations of motion which treat the isothermal constraint differently (for instance by restricting the z temperature alone rather than the average). This comparison shows that the equations of motion (1) used here are consistent with the Chapman-Cowling normal stresses and that the other approaches are not. The computer simulation results in Table 1a are in agreement with this conclusion.

The series in Eqs. (22) and (23) can be generated recursively by calculating moments of the distribution function.⁽¹⁵⁾ The resulting series and numerical results are identical to Zwanzig's calculations, indicating an exact correspondence to all orders in the strain rate between the nonlinear, nonequilibrium distribution functions obtained from the isothermal equations of motion and those derived from a model of a gas enclosed by moving boundaries, heating up due to viscous dissipation. The local equilibrium assumption is common to both calculations. Very recently Evans and Morris have studied transient nonlinear Couette flow,⁽¹⁶⁾ comparing analytically the distribution functions derived from Eqs. (1) and Doll's tensor. They also conclude that Eqs. (1) yield correct normal stresses whereas Doll's tensor does not.

A major remaining problem involves heat conduction. A relaxation time analysis of heat flow (homogeneous, periodic, isothermal, with a constant heat current but no particle current)⁽¹⁷⁾ produces normal stresses which disagree with the Chapman-Cowling analysis.⁽¹⁴⁾ Heat current simulation is also more complicated.⁽¹⁷⁾ The constraints $\sum p = 0$, $\sum p^2$ fixed, $\sum p(p^2)$ fixed require at least three particles, not just one or two.

5. IRREVERSIBILITY⁽¹⁸⁾

The two-dimensional Lorentz gas is the simplest system exhibiting *thermodynamic* irreversibility. The isothermal equations of motion (1) are, however, reversible in time. Thus a movie of the motion, run backward, would still satisfy the equations. This *mathematical* reversibility is not physical, because the reversed movie would exhibit negative viscosity and negative entropy production. As Boltzmann pointed out, the instability of the equations of motion to small perturbations means that the motion can be reversed, with a given accuracy, only at the cost of a precision in the initial conditions which increases *exponentially* in time. The error amplification is easy to see in the Lorentz gas. A small error in the impact parameter db , leads to a corresponding error in the scattering angle, of order db/σ , which leads to an error in the impact parameter at the next collision of order $(\lambda/\sigma) db$, where λ is the free path. Thus, at a density corresponding to a mean free path of ten diameters, approximately one significant figure is lost with every collision. Even very small physical forces destroy reversibility. The gravitational force exerted by the *sun* between two successive collisions of a room temperature molecule of air changes the ratio b/σ by about 1 part in 10^{12} .

The irreversibility which actually occurs can be analyzed more quantitatively for our simple one-body system. Imagine that this system is connected to a physical heat bath, at temperature T , which adds or subtracts

energy as required to keep the temperature of our system constant through the friction coefficient ζ . From the equations of motion, the Coriolis and frictional changes in the comoving particle kinetic energy with time are

$$(d/dt)(p^2/2m) = -\dot{\epsilon}p_x p_y/m + \text{"friction"} = 0 \quad (25)$$

Thus (for $\dot{\epsilon} > 0$) the friction term $+\dot{\epsilon}p_x p_y/m$ contributes energy for momenta in the first or third quadrants and extracts energy in the second and fourth quadrants. The isotropic equilibrium distribution gives no net energy gain or loss. The drift induced by the nonequilibrium equations increases the density in the second and fourth quadrants, leading to a net production of heat, which is then extracted by the thermostat. Thus the streaming motion in velocity space leads to a positive entropy (heat) production.

There is a similar effect in configuration space. In the absence of a strain rate the scattering particle neither gains nor loses energy. In the presence of a moving scatterer as in Fig. 1, the relative inertial-frame speed is increased for collisions in the second and fourth quadrants and decreased in the first and third quadrants. Thus collisions in the first and third quadrants absorb less heat (entropy) than that produced by the more numerous second and fourth quadrant collisions. Because particles moving up tend to collide preferentially in the fourth quadrant, and those moving down collide preferentially in the second, the net effect of collisions is to generate entropy too.

The Lorentz gas features just described are generally valid in many-body systems too. To first order in the strain rate there is no entropy production. There is a positive entropy production which is overestimated by the second-order terms. Both spatial effects, of the kind accounted for approximately by Enskog,⁽¹⁴⁾ and streaming effects contribute to the irreversibility.

6. SUMMARY

The nonequilibrium shear-flow equations of motion can be stably applied to two- and three-dimensional one-body analogs of the Lorentz gas model. This application produces viscosity coefficients exhibiting shear thinning in two or in three dimensions. The Boltzmann equation predicts similar effects though quantitatively somewhat different. This difference is difficult to understand, in light of the similarity in results at both low and high strain rates. The irreversibility inherent in the reversible equations of motion can be analyzed and understood on thermodynamic grounds, by considering heat exchange with a thermostat imposing the isothermal constraint.

ACKNOWLEDGMENTS

Both Jim Dufty (Gainesville) and Denis Evans (Canberra) have been generous with pertinent conversations and preprints. This work was supported, at UC Davis, by the Army Research Office and the Air Force Office of Scientific Research.

APPENDIX A: TRAJECTORIES

Between collisions the equations of motion (1) in the polar coordinate form $\dot{\theta} = \dot{\varepsilon} \sin^2 \theta$, can be integrated (twice) to find x , y , p_x , and p_y as functions of t . With the initial conditions x_0 , y_0 , p_{x0} , p_{y0} at t_0 the solution is

$$\begin{aligned} x &= x_0 + (\tau + c) y_0 + (p/\mu\dot{\varepsilon}) [2(1+c^2)^{1/2} - 2(1+\tau^2)^{1/2} + \tau \ln \psi] \\ y &= y_0 + (p/\mu\dot{\varepsilon}) \ln \psi, \quad \psi \equiv [(1+\tau^2)^{1/2} + \tau]/[(1+c^2)^{1/2} - c] \\ p_x &= -p\tau/(1+\tau^2)^{1/2}, \quad p_y = p/(1+\tau^2)^{1/2} \end{aligned}$$

for $p_y > 0$. For $p_y < 0$ replace p by $-p$ in these equations. The ratio of initial momenta, p_{x0}/p_{y0} , is c ; the relative strain $\dot{\varepsilon}(t-t_0)-c$, is τ .

The Doll's tensor solution is similar. The polar coordinate equation is $\dot{\theta} = -\dot{\varepsilon} \cos^2 \theta$, leading to

$$p_x = p/(1+\tau^2)^{1/2}; \quad p_y = -p\tau/(1+\tau^2)^{1/2}$$

for $p_x > 0$, where $\tau = \dot{\varepsilon}(t-t_0)-c$, with $c = p_{y0}/p_{x0}$

Integrating once more gives

$$\begin{aligned} x &= x_0 + (\tau + c) y_0 + (p/\mu\dot{\varepsilon}) \\ &\quad \times [\tau(1+c^2)^{1/2} - \frac{1}{2}\tau(1+\tau^2)^{1/2} + \frac{1}{2}c(1+c^2)^{1/2} + \frac{1}{2}\ln \psi] \\ y &= y_0 + (p/\mu\dot{\varepsilon}) [(1+c^2)^{1/2} - (1+\tau^2)^{1/2}] \\ \psi &= [(1+\tau^2)^{1/2} + \tau]/[(1+c^2)^{1/2} - c] \end{aligned}$$

REFERENCES

1. E. H. Hauge, in *Transport Phenomena*, G. Kirczenow and J. Marro, eds., Springer Lecture Notes in Physics, No. 31 (Springer, New York, 1974), p. 337.
2. E. G. D. Cohen, Colloques Internationaux CNRS No. 236, Théories cinétiques classiques et relativistes, p. 269.
3. C. Bruin, *Physica* **72**:261 (1974).
4. W. W. Wood and F. Lado, *J. Comp. Phys.* **7**:528 (1971).
5. W. E. Alley, Ph. D. dissertation, University of California, Davis, California (1981).

6. W. G. Hoover, *Physica* **118A**:111 (1983).
7. B. L. Holian and D. J. Evans, *J. Chem. Phys.* **78**:5147 (1983).
8. B. L. Holian, W. G. Hoover, B. Moran, and G. K. Straub, *Phys. Rev. A* **22**:2798 (1980).
9. H. J. M. Hanley, ed. *Nonlinear Fluid Behavior*, Proceedings of the Conference on Non-linear Fluid Behavior held at University of Colorado at Boulder, June 7-11, 1982, in *Physica* **118A** (1983).
10. D. J. Evans and G. P. Morriss, *Computer Phys. Rep.* **1**:297 (1984).
11. W. G. Hoover, D. J. Evans, R. B. Hickman, A. J. C. Ladd, W. T. Ashurst, and B. Moran, *Phys. Rev. A* **22**:1690 (1980).
12. D. M. Gass, *J. Chem. Phys.* **54**:1898 (1971).
13. R. W. Zwanzig, *J. Chem. Phys.* **71**:4416 (1979); M. C. Marchetti and J. W. Dufty, *J. Stat. Phys.* **32**:255 (1983).
14. S. Chapman and T. G. Cowling, *The Mathematical Theory of Non-Uniform Gases* (Cambridge University Press, Cambridge, England, 1939).
15. A. J. C. Ladd, unpublished.
16. D. J. Evans and G. P. Morriss, *Phys. Rev. A* **30**:1528 (1984).
17. D. J. Evans, *Phys. Lett.* **91A**:457 (1982); W. G. Hoover, B. Moran, and J. M. Haile, *J. Stat. Phys.* **37**:109 (1984).
18. W. G. Hoover, K. A. Winer, and A. J. C. Ladd, *Int. J. Eng. Sci.* (in press).